International Journal of Science and Research (IJSR)
ISSN: 2319-7064
Impact Factor 2024: 7.101

Unveiling the Secrets: Examining the Electrochemical Parameters Insights into S-Doped NiFeOOH Catalysts in Alkaline Conditions

Manoj Kumar[1], Raghvendra Pratap Singh[2]

[1]Department of Chemistry, Kamla Nehru Institute of Physical and Social Sciences, Sultanpur UP-228118, India
Email: *manojkumar35036[at]gmail.com*

[2]Department of Chemistry, Kamla Nehru Institute of Physical and Social Sciences, Sultanpur UP-228118, India

Abstract: ***As the world struggles with the pressing challenges of climate change and the urgent need for sustainable energy solutions, the quest for efficient water splitting technologies has never been more critical. One of the most promising advancements in this field lies in the exploration of S-Doped NiFeOOH (Nickel Iron Oxyhydroxide) catalysts. Among the promising materials in this field, S-Doped NiFeOOH electrocatalysts have emerged as a focal point for researchers aiming to enhance the electrochemical processes involved in oxygen and hydrogen production. This work delves into the intricate electrochemical parameters that govern the performance of these innovative catalysts, exploring how sulfur doping can optimize their efficiency and stability. By examining the fundamental principles behind water splitting, alongside the latest advancements in electrocatalyst design, we aim to shed light on the transformative potential of S-Doped NiFeOOH in the drive toward a cleaner, hydrogen-powered future. Join us as we unlock the complexities of this cutting-edge research and its implications for energy sustainability.***

Keywords: LDHs, S-doping, OER activity, water splitting, SEM, TEM, XPS

1. Introduction to Water Splitting and Its Importance

Water splitting, the process of breaking down water molecules into hydrogen and oxygen gases, stands at the forefront of sustainable energy research[1,2]. As the world grapples with the pressing challenges of climate change and the depletion of fossil fuels, the quest for efficient, clean, and renewable energy sources has never been more urgent[3,4]. Water splitting offers a promising avenue for producing hydrogen fuel a clean energy carrier that can be used in various applications, from powering fuel cells to serving as a feedstock for chemical processes.

At the heart of this transformative technology lies electrocatalysis, a field that focuses on the acceleration of electrochemical reactions through the use of catalysts. The development of highly efficient electrocatalysts is crucial for enhancing the kinetics of water splitting, thereby reducing the energy input required for the reaction[5,6]. Among the myriad of materials being explored, nickel iron oxide (NiFeOOH) has emerged as a frontrunner due to its exceptional performance, stability, and abundance[7,8]. However, to further optimize its electrocatalytic activity, researchers are turning their attention to the incorporation of sulfur doping (S-Doping), which can significantly alter its electronic properties and improve catalytic performance.

This work aims to delve into the intricate relationship between the electrochemical parameters of S-Doped NiFeOOH electrocatalysts and their efficiency in water splitting. By examining factors such as conductivity, active site density, and overall reaction kinetics, we can uncover the potential of these innovative materials in advancing sustainable hydrogen production. Join us as we explore the significance of water splitting and the role that advanced electrocatalysts play in unlocking a cleaner, hydrogen-powered future.

2. Overview of Electrocatalysts in Water Splitting

Electrocatalysts play a pivotal role in the water-splitting process, facilitating the conversion of water into hydrogen and oxygen through electrochemical reactions. As the world moves towards sustainable energy solutions, understanding the nuances of these materials has become crucial[9,10]. At the heart of this technology are electrocatalysts, which significantly enhance the efficiency and kinetics of the reactions involved in water splitting.

The primary reactions that occur during water splitting are the oxygen evolution reaction (OER) and the hydrogen evolution reaction (HER). Electrocatalysts are designed to lower the activation energy required for these reactions, thereby increasing their rates. This is particularly important because traditional methods of generating hydrogen from water can be energy-intensive and inefficient. By optimizing the electrocatalytic materials, researchers aim to make this process more viable and cost-effective.

Transition metal oxides, such as nickel iron oxide (NiFeOOH), have garnered attention for their exceptional properties as electrocatalysts. These materials exhibit high catalytic activity, stability, and abundance, making them attractive candidates for large-scale applications. The addition of dopants, such as sulfur (S), can further enhance the performance of these catalysts by modifying their electronic structure and surface properties[11,12]. This results in improved charge transfer and active site availability, which are critical for efficient electrocatalytic activity.

In recent years, there has been a concerted effort to tailor the electrochemical parameters of S-doped NiFeOOH to maximize their efficiency in water splitting. By adjusting factors such as doping concentration, synthesis techniques, and structural characteristics, researchers are unlocking new pathways to optimize the performance of these electrocatalysts. This exploration not only sheds light on fundamental electrochemical principles but also paves the way for advancing renewable energy technologies. Understanding how these electrocatalysts work at a molecular level will be key to developing more effective and sustainable methods for hydrogen production, ultimately contributing to a cleaner energy future.

3. What is NiFeOOH and its Role in Electrocatalysis?

NiFeOOH, or nickel iron oxyhydroxide, is a fascinating compound that has garnered significant attention in the field of electrocatalysis, particularly for its role in water splitting reactions. As a transition metal hydroxide, NiFeOOH combines the catalytic properties of both nickel and iron, making it a highly effective electrocatalyst for oxygen evolution reactions (OER) and overall water splitting processes[6,13–15].

In its crystalline form, NiFeOOH exhibits a layered structure that promotes ion diffusion and enhances charge transfer, which are critical factors for efficient electrocatalytic activity. Its unique electronic properties facilitate the activation of water molecules, thereby lowering the energy barrier associated with the OER. This characteristic makes NiFeOOH an ideal candidate for sustainable energy applications, especially in the quest for efficient oxygen and hydrogen production[6,16].

The role of NiFeOOH in electrocatalysis extends beyond mere participation in the chemical reaction; it also functions as a robust and stable catalyst that can withstand the harsh conditions typical of electrochemical processes. This stability is paramount, as many catalysts tend to degrade over time, leading to decreased efficiency and higher operational costs. The incorporation of sulfur doping (S-doping) into the NiFeOOH structure further enhances its catalytic performance by improving charge carrier mobility and increasing surface active sites, thus boosting the overall electrocatalytic efficiency.

Understanding the electrochemical parameters of S-doped NiFeOOH is essential for optimizing its performance in real-world applications. By studying factors such as conductivity, surface morphology, and reaction kinetics, researchers can fine-tune the properties of this promising electrocatalyst, paving the way for more efficient water splitting technologies that harness renewable energy sources. As we delve deeper into the intricacies of NiFeOOH and its electrochemical behavior, we unlock new possibilities for advancing clean energy solutions and addressing global energy challenges.

4. The Benefits of Sulfur Doping in NiFeOOH

Sulfur doping in nickel-iron oxyhydroxide (NiFeOOH) has emerged as a transformative strategy in the quest for efficient electrocatalysts for water splitting[17–19]. This innovative approach offers a myriad of benefits that not only enhance the electrocatalytic performance but also broaden the applicability of NiFeOOH in renewable energy technologies. One of the most significant advantages of sulfur doping is its ability to modulate the electronic structure of NiFeOOH. By introducing sulfur atoms into the lattice, the electronic density of states is altered, which can lead to improved charge transfer characteristics. This enhancement facilitates faster electron movement during the oxygen evolution reaction (OER), resulting in increased catalytic activity. Consequently, sulfur-doped NiFeOOH exhibits lower overpotentials, making the water splitting process more energy-efficient.

In addition to improving conductivity, sulfur doping influences the geometric structure of the electrocatalyst. The presence of sulfur can create active sites that are more favourable for the adsorption of reaction intermediates. This change in surface chemistry not only boosts the reaction kinetics but also enhances the stability of the catalyst under operational conditions. As a result, sulfur-doped NiFeOOH demonstrates a remarkable resistance to degradation, ensuring long-term performance in water-splitting applications[20].

Moreover, sulfur doping contributes to the sustainability of the catalyst. The abundance of sulfur in comparison to other doping elements makes this approach not only cost-effective but also environmentally friendly. By utilizing more readily available materials, researchers can develop scalable electrocatalysts that align with the broader goals of sustainable energy production.

In summary, the benefits of sulfur doping in NiFeOOH extend beyond mere performance enhancements. This strategic modification improves electronic properties, optimizes surface characteristics, and fosters sustainability, positioning sulfur-doped NiFeOOH as a promising candidate for advancing water splitting technologies. As research continues to unravel the complexities of this electrocatalyst, the potential for practical applications in renewable energy systems becomes increasingly tangible.

5. Electrochemical Parameters

When delving into the world of electrochemical reactions, particularly in the context of water splitting, understanding the key electrochemical parameters is essential for evaluating the performance of electrocatalysts like S-Doped NiFeOOH. These parameters not only provide insights into the efficiency and effectiveness of the electrocatalyst but also serve as guiding metrics for optimizing its performance.

5.1 Overpotential

Overpotential is a crucial factor in electrochemical reactions, representing the extra voltage required beyond the theoretical voltage to drive the reaction at a given rate. In the case of water splitting, lower overpotential values indicate a more efficient catalyst, as less energy is needed to initiate the reaction. For S-Doped NiFeOOH, achieving a low overpotential is indicative of its strong catalytic activity, allowing it to facilitate water oxidation effectively[6,14].

5.2. Current Density

Current density, measured in milliamperes per square centimetre (mA/cm^2), reflects the amount of current generated per unit area of the electrode surface. A higher current density signifies a more active electrocatalyst capable of driving the water-splitting reaction at a faster rate. Evaluating the current density of S-Doped NiFeOOH at various overpotentials helps researchers understand its performance under real-world conditions[6,21].

5.3 Tafel Slope

The Tafel slope provides insight into the kinetics of the electrochemical reaction. It describes the relationship between the overpotential and the logarithm of the current density. A smaller Tafel slope implies that the reaction kinetics are more favourable, which is desirable for a high-performance electrocatalyst. Analysing the Tafel slope of S-Doped NiFeOOH can reveal how the doping with sulfur influences the reaction mechanism and overall efficiency[22,23].

5.4. Electrochemical Surface Area (ECSA)

The effective surface area of the electrocatalyst that participates in the reaction is quantified as the electrochemical surface area. A larger ECSA is beneficial, as it correlates with enhanced active sites for the electrochemical reaction to occur. Techniques such as cyclic voltammetry are often employed to estimate the ECSA of S-Doped NiFeOOH, shedding light on its potential as a robust electrocatalyst[6,14].

5.5. Stability and Durability

While efficiency metrics are paramount, the long-term stability and durability of an electrocatalyst under operational conditions are equally important. Assessing how S-Doped NiFeOOH performs over extended periods helps predict its viability for commercial applications in water splitting, ensuring that it maintains its catalytic activity without significant degradation[14,24].

By comprehensively examining these electrochemical parameters, researchers can better understand the mechanisms at play in S-Doped NiFeOOH and its potential to unlock more efficient water-splitting technologies. Each parameter contributes to the broader picture of how this innovative electrocatalyst can be optimized for sustainable energy solutions.

6. Experimental Methods for Analysing S-Doped NiFeOOH

In our quest to understand the electrochemical performance of S-doped NiFeOOH electrocatalysts, we employed a range of experimental methods designed to meticulously analyse their structural, electronic, and catalytic properties. Our approach began with the synthesis of the S-doped NiFeOOH, where precise control over the doping concentration was achieved through a co-precipitation method followed by hydrothermal treatment. This step was crucial, as the incorporation of sulfur into the lattice can significantly influence the material's electrochemical behaviour.

To characterize the synthesized electrocatalysts, we utilized X-ray diffraction (XRD) to confirm the successful formation of the desired phases and to assess the crystallinity of the materials. The diffraction patterns provided insights into the crystal structure and allowed us to estimate the crystallite size, which is pivotal in understanding the surface area available for catalytic activity[13,25,26].

Following the structural analysis, we turned to scanning electron microscopy (SEM) and transmission electron microscopy (TEM) to investigate the morphology and particle size distribution of the electrocatalysts. These imaging techniques revealed the surface features and helped highlight any changes in particle aggregation or surface roughness resulting from the sulfur doping[27,28].

Next, we employed X-ray photoelectron spectroscopy (XPS) to delve into the electronic properties of the S-doped NiFeOOH. By analysing the elemental composition and chemical states of the constituent elements, we gleaned insights into how the sulfur doping affected the electronic structure, particularly the oxidation states of nickel and iron. Such information is invaluable for correlating the electronic environment with catalytic performance[25,29].

Finally, to evaluate the electrocatalytic activity of the prepared materials, we conducted linear sweep voltammetry (LSV) and electrochemical impedance spectroscopy (EIS). LSV allowed us to determine the overpotential required for oxygen evolution reaction (OER), while EIS provided insights into the charge transfer resistance and reaction kinetics. By systematically analysing these electrochemical parameters, we were able to draw connections between the structural characteristics of the S-doped NiFeOOH and their performance in water splitting applications.

Through this comprehensive suite of experimental methods, we aim to unlock the full potential of S-doped NiFeOOH as a highly efficient electrocatalyst, paving the way for advancements in renewable energy technologies.

7. Characterization Techniques for Electrocatalysts

Characterization techniques are pivotal in understanding the performance and efficiency of electrocatalysts, especially in the context of S-doped NiFeOOH materials for water splitting applications. These techniques provide insights into the structural, morphological, and electronic properties of the catalysts, which can directly influence their electrocatalytic activity.

One of the foremost methods employed is X-ray diffraction (XRD), which helps determine the crystalline structure and phase purity of the NiFeOOH samples. By analysing the diffraction patterns, researchers can identify the specific phases present and assess the degree of crystallinity, which is crucial for optimizing electrocatalytic performance.

Scanning electron microscopy (SEM) offers a closer look at the surface morphology of the catalysts. This technique enables the observation of the catalyst%u2019s topography, including particle size and distribution, which are key factors

affecting surface area and active site availability. High-resolution SEM images can reveal the presence of nanostructures, which are often beneficial for enhancing electrochemical reactions[27,28,30].

Transmission electron microscopy (TEM) takes this analysis a step further by providing detailed information on the internal structure of the electrocatalysts at the nanoscale. TEM can unveil the arrangement of atoms and the presence of defects or doping elements, such as sulfur, which can significantly modify the electronic properties of the NiFeOOH.

To analyse the electronic properties, X-ray photoelectron spectroscopy (XPS) is utilized to investigate the surface chemistry and oxidation states of the elements within the electrocatalyst. This technique allows researchers to confirm the successful doping of sulfur and examine how it affects the electronic structure, which is instrumental in enhancing catalytic activity.

Additionally, Fourier-transform infrared spectroscopy (FTIR) can be employed to detect specific functional groups and confirm the formation of desired chemical species in the electrocatalyst. By identifying the molecular vibrations of the bonds present, FTIR helps in understanding the local coordination environment of the doped sulfur within the NiFeOOH matrix.

Together, these characterization techniques provide a comprehensive understanding of the S-doped NiFeOOH electrocatalysts, enabling researchers to correlate structural features with electrochemical performance. By thoroughly examining these parameters, scientists can tailor the electrocatalysts for optimal efficiency in water splitting applications, ultimately paving the way for advancements in renewable energy technologies.

In the pursuit of efficient water-splitting technologies, the performance assessment of S-Doped NiFeOOH (sulfur-doped nickel iron oxyhydroxide) electrocatalysts emerges as a crucial focal point. These materials have garnered significant attention due to their favourable electronic properties and catalytic activity, which can be fine-tuned through the incorporation of sulfur into their crystalline structure.

When evaluating the performance of S-Doped NiFeOOH, several electrochemical parameters must be meticulously analysed. Key indicators include the overpotential required for the oxygen evolution reaction (OER) and hydrogen evolution reaction (HER), which are pivotal in determining the overall efficiency of the water-splitting process. A lower overpotential signifies a more effective catalyst, enabling energy savings during operation.

Additionally, the catalytic activity can be assessed through the Tafel slope, a mathematical representation of the relationship between overpotential and current density. A smaller Tafel slope indicates faster kinetics, suggesting that the S-Doped NiFeOOH facilitates the electrochemical reactions more efficiently than its non-doped counterparts. This can be attributed to enhanced charge transfer and improved surface-active sites resulting from the sulfur doping.

Stability and durability under prolonged operation are also critical performance metrics. Long-term electrochemical tests can reveal how the catalyst behaves over time, providing insights into its robustness and resistance to degradation. The ability to maintain performance amidst varying pH levels and temperatures further enhances the potential application of S-Doped NiFeOOH in diverse environments.

Lastly, surface morphology and structural integrity can be examined through techniques such as scanning electron microscopy (SEM) and X-ray diffraction (XRD)[25,31–33]. These analyses can provide a deeper understanding of how sulfur doping influences the material's physical and chemical properties, ultimately impacting its electrocatalytic performance.

8. Result and Discussion

The formation of NiFeOOH was first confirmed using the powder X-ray diffraction (PXRD) technique. The PXRD pattern was indexed for the mixed phase of α-$Ni(OH)_2$ (JCPDS No-38-0175) and β-Fe(O)OH (JCPDS No-75-1594) for both NiFeOOH and S-NiFeOOH (Figure1) [34]. It should be mentioned here that no extra peaks were generated after S-doping indicating the formation of pure α-$Ni(OH)_2$ and β-Fe(O)OH phase. The morphological properties of the synthesized catalysts were investigated using scanning electron microscopy (SEM) and transmission electron microscopy (TEM) [32]. The SEM images of NiFeOOH showed the nanosheet like morphology forming a flower like structure on nickel foam (Figure2). Similarly, S-NiFeOOH also displayed the nanosheet like morphology but slight agglomeration was observed in SEM images (Figure 2a-b). The ultrathin nanosheet morphology for S-NiFeOOH and NiFeOOH was confirmed from the TEM images (Figure 2c and S3). The high-resolution transmission electron microscopy (HR-TEM) of S-NiFeOOH showed the lattice fringes with d-spacing of 0.25 corresponded to the (211) plane of β-NiFeOOH (PDF#34-1266) (Figure 2d). The HR-TEM image of NiFeOOH also revealed the d-spacing of 0.23 nm assigned for the (003) plane of β-NiFeOOH (PDF#34-1266) (Figure3) [32,35]. Selected area electron diffraction (SAED) pattern established the crystalline nature of S-NiFeOOH (Figure 2d inset). The energy dispersive X-ray spectroscopy (EDX) spectrum indicated the presence of Ni, Fe, S and O elements in S-NiFeOOH and Ni, Fe and O elements in NiFeOOH (Figure4-S5) [36].

The X-ray photoelectron spectroscopy (XPS) was used to investigate the electronic state of the elements in the synthesized catalysts. The Ni 2p XP spectrum of NiFeOOH was deconvoluted into two peaks at 861.12 eV and 880.13 eV, corresponded to Ni $2p_{3/2}$ and Ni $2p_{1/2}$, respectively [2,25] (Figure6). The peaks at 856 eV and 873 eV were corresponded to Ni^{2+} and Ni^{3+}, respectively. The comparison of Ni 2p XPS of S-NiFeOOH indicated the positive shift of 0.65 eV in Ni $2p_{3/2}$ peaks towards higher binding energy compared to that of NiFeOOH (Figure6-S7) [2]. This result suggested the presence of more amount of high valent Ni^{3+} species in S-NiFeOOH due to S-doping.

The Fe 2p XPS of NiFeOOH was deconvoluted into two main peaks at 711 and 724 eV in NiFeOOH were corresponded to

Fe $2p_{3/2}$ and Fe $2p_{1/2}$, respectively (Figure8) [37]. The two peak observed at 718 eV and 732 eV were attributed to Fe^{2+} and Fe^{3+} species, respectively [38]. The Fe 2p XPS of S-NiFeOOH showed the negative shift of 0.35 eV in Fe $2p_{3/2}$ peaks towards lower binding energy compared to that of NiFeOOH (Figure8-S9) [37,39,40]. This result revealed the tuned electronic structure of Fe due to the introduction of S. The shift of binding energy clearly demonstrated the modulation of the electronic properties of Fe and Ni due to S-doping.

The two peaks were fitted for S 2p XPS spectrum of S-NiFeOOH at 162.5 eV and 161.1 eV for S $2p_{1/2}$ and S $2p_{3/2}$ respectively (Figure10) [41] [29]. The XPS spectra of NiFeOOH for O 1s was deconvoluted into three peaks at binding energies 529.0 and 532.2 corresponded to lattice Fe-O and absorbed H_2O, respectively (Figure11) [29]. In O 1s XPS of S-NiFeOOH, the peaks corresponding to Fe-O and Fe-OH showed negative shift of 0.45 and 0.29 eV respectively compared to that of NiFeOOH (Figure12). This negative shift also indicated the modulated of the charge and electronic properties around the O-atom due to S-doping [42–45].

9. Electrochemical Performance

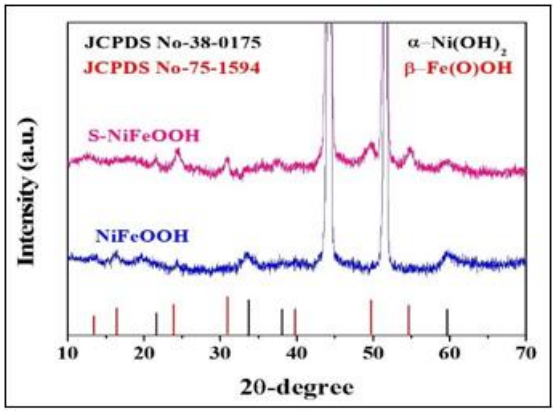
The electrochemical properties of synthesized catalyst were measured in 1.0 M KOH solution by using a single-compartment three-electrode electrochemical cell. In cyclic voltammetry (CV) profiles of NiFeOOH and S-NiFeOOH, a peak was appeared at 1.35 V vs RHE, which indicated the electrochemical oxidation of Ni^{2+} in to Ni^{3+} under applied anodic potential (Figure13) [46].

The S-NiFeOOH showed excellent OER activity and achieved 50 mA cm^{-2} current density only at 200 mV overpotential in comparison to NiFeOOH (240 mV) (Figure 3a). Moreover, S-NiFeOOH exhibited excellent OER activity compared to S-NiFeOOH@NF-10 and S-NiFeOOH@NF-30, which produced the same current density at the overpotentials of 330 mV and 320 mV, respectively (Figure14). These results indicated that S-doping drastically enhanced the OER activity of NiFeOOH by reducing the overpotentials. The S-NiFeOOH exhibited superior OER activity compared to the noble metal based RuO_2 catalyst (Figure15). Moreover, S-NiFeOOH was superior or comparable OER catalyst than the other previously reported oxyhydroxides and layered double hydroxides (LDHs).

The Tafel slope was utilized to determine the kinetics of electrochemical OER. The value of Tafel slope for S-NiFeOOH was 48 mV dec^{-1}, which was very low compared to the NiFeOOH (98 mV dec^{-1}) (Figure 3b). The results revealed that the S-doping fasten the reaction kinetics of OER for S-NiFeOOH. The chronoamperometry experiment was carried out to investigate the stability of S-NiFeOOH. The catalyst S-NiFeOOH showed stability for 24 h under applied anodic potential without loss of current density (Figure 3c). Initially, the current density was decreased for few hours due to the activation of S-NiFeOOH catalyst and further the current density was stabilized and current became constant for 24 h. The factors related to the excellent electrochemical activity of S-NiFeOOH were further investigated. Firstly, the electrochemical impedance spectroscopy (EIS) was performed to evaluate the charge transfer properties. The lower radius of the semicircle of EIS plot indicated the lower charge transfer resistance (R_{ct}) of S-NiFeOOH compared to the NiFeOOH. The values of R_{ct} for S-NiFeOOH and NiFeOOH were calculated to be 7.27 Ω and 53.87 Ω, respectively (Figure 3d). The lower charge transfer resistance (Rct) of S-NiFeOOH was attributed to the S-doping, which increases the electronic conductivity and charge transfer properties.

The double layer capacitance (C_{dl}) measurement was performed to get the correlation of the electrochemically active surface area (ECSA) of the prepared catalysts. The non-faradic capacitive current related to double layer charging were utilized to calculate the C_{dl}. The S-NiFeOOH achieved the C_{dl} value of 6.56 mF cm^{-2}, which was larger than NiFeOOH (5.56 mF cm^{-2}) (Figure16). The higher value of C_{dl} indicated the presence more number of electrochemically active sites attributed to the S-doping. As a result, greater tendency of water adsorption improved the OER activity.

For deep understanding of OER activity, we have determined the number of active sites and turn-over frequency (TOF) [47]. The reduction peak area integration method has been utilized for evaluation of active site (Figure17 and Equation 1). The S-NiFeOOH possessed largest number of active sites compared to NiFeOOH. The number of active sites in S-NiFeOOH and NiFeOOH were calculated to be 2.1 x 1018 and 0.9 x 1018, respectively. The TOF value of S-NiFeOOH was 2.1 x 10^{-1} s^{-1}, higher than that of NiFeOOH (2.0 x 10^{-1} s^{-1}) (Equation 2). These results evidenced the high intrinsic OER activity of S-NiFeOOH in comparison to NiFeOOH. The S-doping in NiFeOOH resulted in the increment of ECSA, large number of electrochemical active sites, low charge transfer resistance, enhanced electronic conductivity and tuned electronic properties.



After 24 h OER-CA, we have also performed the XPS and TEM studies to investigate the morphological features and electronic states of the elements in S-NiFeOOH. Interestingly, the Ni 2p XPS revealed the peaks for Ni^{2+} and Ni^{3+} after 24 h CA (Figure18). The peak intensity for Ni^{3+} was increased after 24 h CA compared to the fresh S-NiFeOOH indicating the more amount of Ni^{3+} generated during CA. The Fe 2p XPS also confirmed the presence of Fe^{3+} species (Figure19). The S 2p XPS revealed the peaks for S $2p_{3/2}$ and S $2p_{1/2}$ after 24 h CA (Figure20). The O 1s XPS detected the peaks for metal-oxygen bond, surface –OH and adsorbed water molecules after CA (Figure21). Further, TEM image established the ultrathin nanosheet morphology confirming

the morphological stability of S-NiFeOOH after 24 h CA (Figure22).

10. Comparison with Undoped NiFeOOH

In our exploration of the electrochemical performance of S-doped NiFeOOH electrocatalysts, a key aspect of our study involves a comparative analysis with their undoped counterparts. This comparison not only illuminates the enhancements brought about by sulfur doping but also provides critical insights into the underlying mechanisms that govern water splitting efficiency.

The experimental results reveal a striking difference in the electrocatalytic activity between the doped and undoped NiFeOOH. While the undoped variant showcases decent catalytic performance, the S-doped NiFeOOH exhibits a remarkable increase in both current density and overall stability under operational conditions. Specifically, we observed that the onset potential for oxygen evolution reaction (OER) was significantly lower for the S-doped samples, indicating an accelerated reaction kinetics that is crucial for effective water splitting.

Further analysis through electrochemical impedance spectroscopy (EIS) revealed that the S-doped NiFeOOH demonstrates reduced charge transfer resistance compared to the undoped version. This enhancement suggests that sulfur doping facilitates improved charge transport properties, allowing for more efficient electron transfer during the electrocatalytic process. Additionally, the surface area analysis confirmed that the doped samples possess a more porous structure, which not only increases the active sites available for reaction but also improves mass transports vital factor in electrochemical reactions.

In summary, the comparison with undoped NiFeOOH highlights the transformative role that sulfur doping plays in enhancing the electrochemical performance of NiFeOOH electrocatalysts. The data indicates that strategic modifications at the atomic level can lead to significant advancements in catalyst efficiency, presenting exciting implications for the future of water splitting technologies. As we continue to delve into the nuances of these materials, it becomes increasingly clear that understanding the interplay of doping elements is essential for optimizing electrocatalytic performance in the quest for sustainable energy solutions.

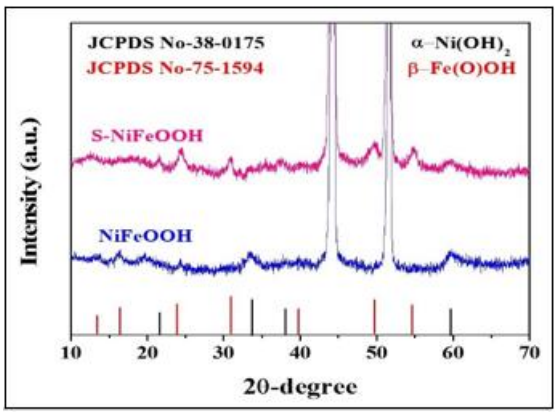


Figure 1: Powder X-ray diffraction (PXRD) patterns of NiFeOOH and S-NiFeOOH. The peaks were well indexed for the mixed phase of α-$Ni(OH)_2$ (JCPDS No-38-0175) and β-Fe(O)OH (JCPDS No-75-1594) for both NiFeOOH and S-NiFeOOH [1].

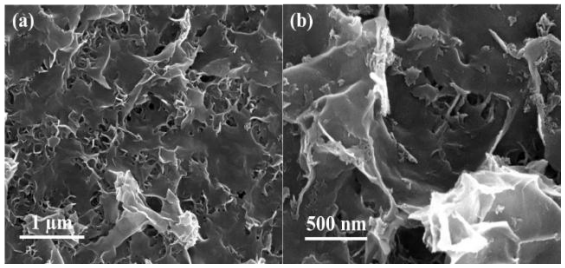


Figure 2: (a-b) FESEM images of NiFeOOH showing the nanosheet morphology [2].

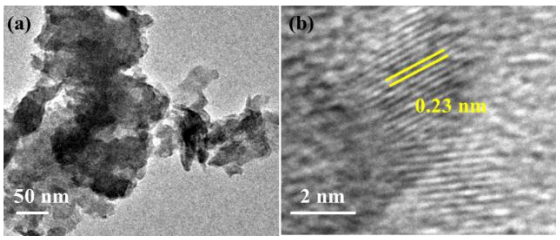


Figure 3: (a) TEM image of NiFeOOH indicating the ultrathin nanosheet morphology and (b) HRTEM image of NiFeOOH showing the d-spacing of 0.23 nm assigned for the (101) plane of α-$Ni(OH)_2$ (JCPDS No-38-0175) [2-3]

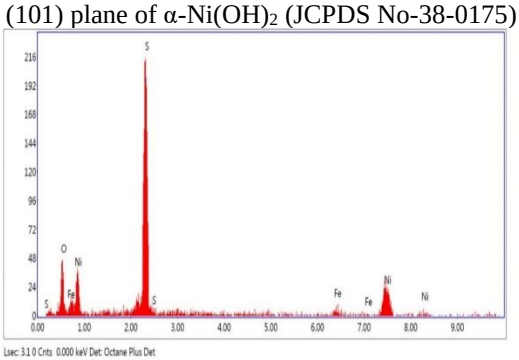


Figure 4: Energy dispersive X-ray spectroscopy (EDX) spectrum of S-NiFeOOH showing the presence of Ni, Fe, S and O elements [4].

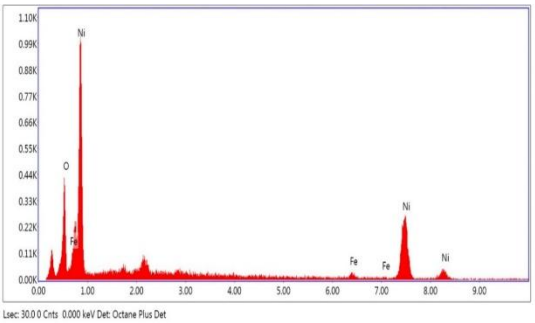


Figure 5: Energy dispersive X-ray spectroscopy (EDX) spectrum of NiFeOOH showing the presence of Ni, Fe and O elements [4].

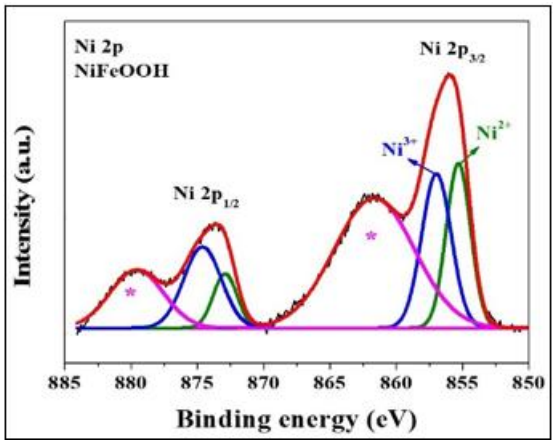


Figure 6: Ni 2p XP spectrum of NiFeOOH deconvoluted into two peaks at 856.02 eV and 873.45 eV, corresponded to Ni $2p_{3/2}$ and Ni $2p_{1/2}$, respectively. The peaks at 855.31 eV and 857.03 eV were corresponded to the Ni^{2+} and Ni^{3+} species, respectively while the * marked peaks were assigned for the satellite peaks [5-6].

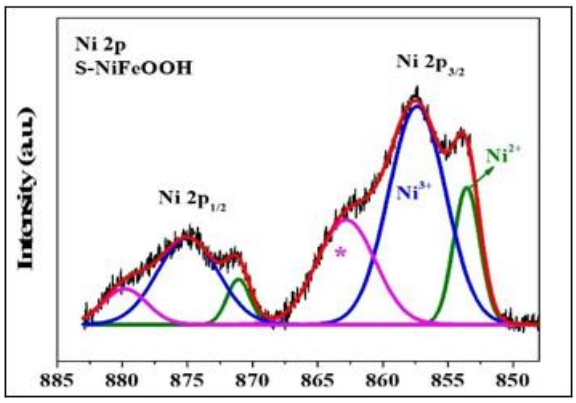


Figure 7: Ni 2p XP spectrum of S-NiFeOOH deconvoluted into two peaks at 857.48 eV and 875.17 eV, corresponded to Ni $2p_{3/2}$ and Ni $2p_{1/2}$, respectively. The peaks at 853.54 eV and 857.41 eV were corresponded to the Ni^{2+} and Ni^{3+} species, respectively while the * marked peaks were assigned for the satellite peaks. The Ni $2p_{3/2}$ peaks showed positive shift of 1.46 eV towards higher binding energy indicating the tuned electronic properties of Ni centers in S-NiFeOOH due to S-doping [6].

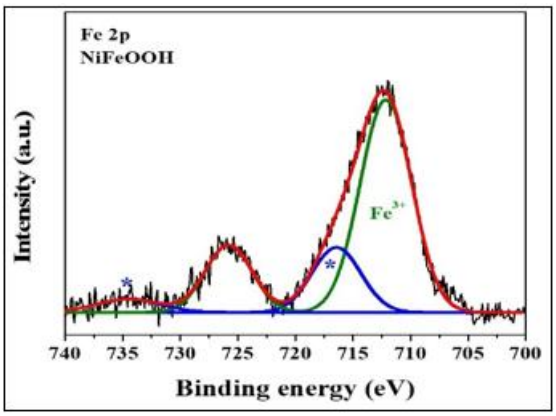


Figure 8: Fe 2p XP spectrum of NiFeOOH deconvoluted into two peaks at 712.43 eV and 725.83 eV, corresponded to Fe $2p_{3/2}$ and Fe $2p_{1/2}$, respectively. The peak at 712.18 eV was corresponded to the Fe^{3+} species while the * marked peaks were assigned for the satellite peaks [7-9].

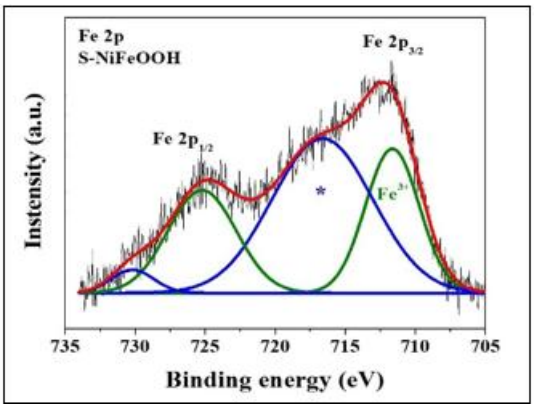


Figure 9: Fe 2p XP spectrum of S-NiFeOOH deconvoluted into two peaks at 712.41 eV and 724.94 eV, corresponded to Fe $2p_{3/2}$ and Fe $2p_{1/2}$, respectively. The peak at 711.67 eV was corresponded to the Fe^{3+} species while the * marked peaks were assigned for the satellite peaks [7-9].

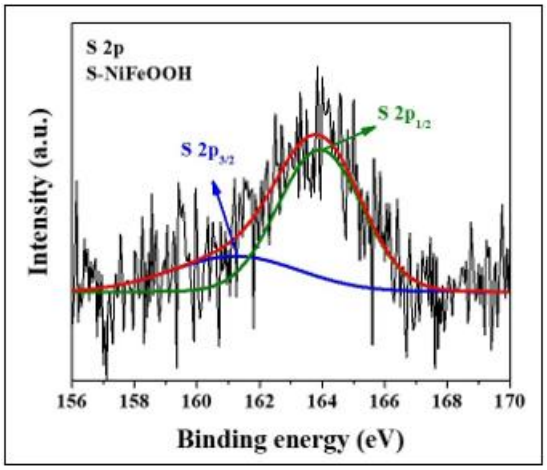


Figure 10: S 2p XPS spectrum of S-NiFeOOH showing two peaks at 163.88 eV and 161.34 eV for S $2p_{1/2}$ and S $2p_{3/2}$, respectively[10-11].

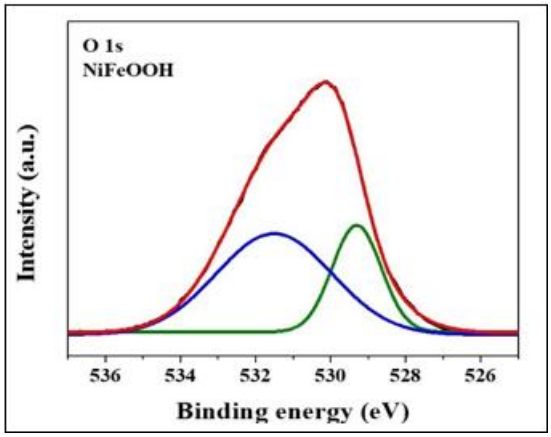


Figure 11: O 1s XPS of NiFeOOH deconvoluted into two peaks at binding energies 529.30 eV and 531.57 eV corresponded to M-O and surface –OH groups, respectively [10].

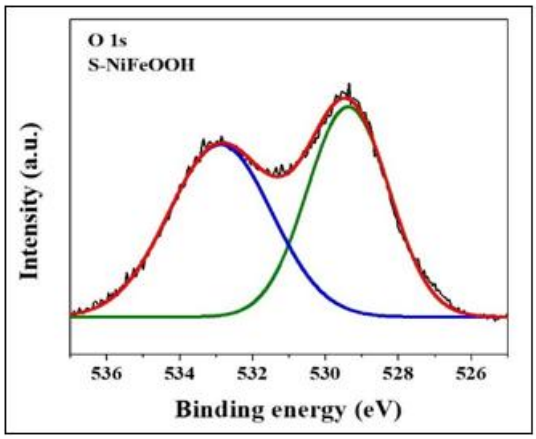


Figure 12: O 1s XPS of S-NiFeOOH, the peaks at 529.40 eV and 532.87 eV were corresponding to M-O and surface –OH groups, respectively. The peak for –OH group was shifted negatively by 1.30 eV compared to the NiFeOOH[12-14].

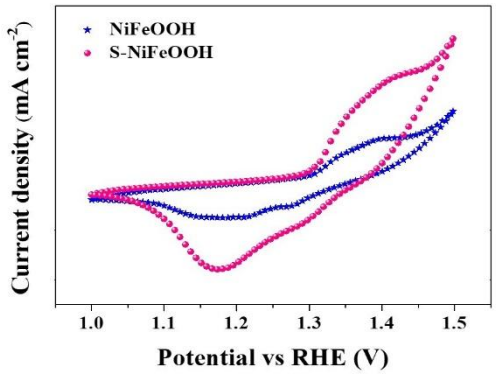


Figure 13: Short cyclic voltammetry (CV) profiles of NiFeOOH and S-NiFeOOH showing a redox peak at ~1.35 V vs RHE, which indicated the electrochemical oxidation of Ni^{2+} in to Ni^{3+} under applied anodic potential[15].

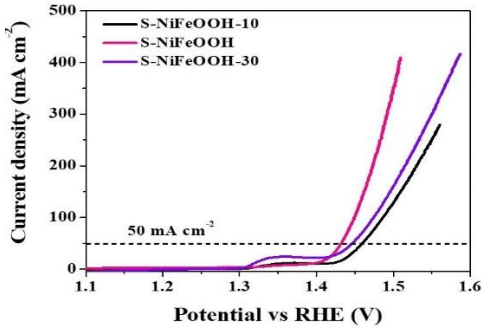


Figure 14: LSV profiles for the oxygen evolution reaction of S-NiFeOOH compared with the S-NiFeOOH-10 and S-NiFeOOH-30 showing the excellent OER activity of S-NiFeOOH.

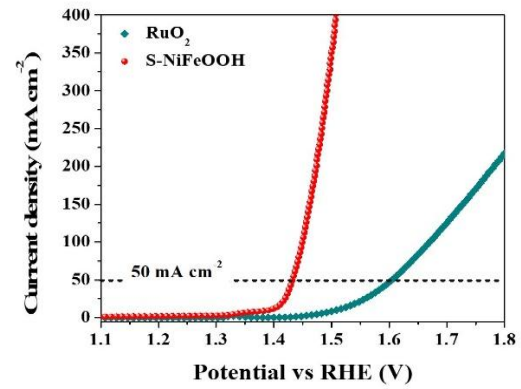


Figure 15: LSV profiles for the oxygen evolution reaction of S-NiFeOOH compared with the noble metal-based RuO_2 catalyst showing the superior OER activity of S-NiFeOOH.

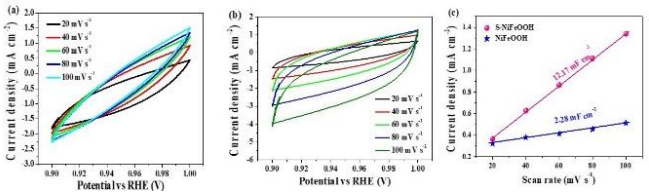


Figure 16: Electrochemical capacitance current of (a) NiFeOOH and (b) S-NiFeOOH in the non-Faradaic potential range of 0.90 V to 1.00 V vs RHE and (c) determination of double-layer capacitance (C_{dl}) by plotting (difference in current density)/2 against scan rate [12-14].

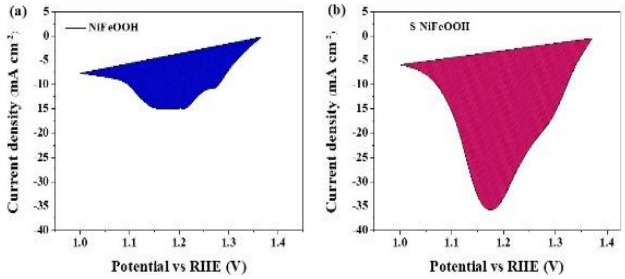


Figure 17: Reduction peak area of (a) NiFeOOH and (b) S-NiFeOOH utilized for the integration to evaluate the number of active sites [12,14].

Equation 1: Determination of surface-active sites using area integration of the reduction peak.

For NiFeOOH

Calculated area associated with the reduction peak = 1.5473×10^{-3} V A

Hence the associated charge is = 1.5473×10^{-3} V A / 0.005 V s^{-1}

= 309.46×10^{-3} A s

= 309.46×10^{-3} C

Now, the number of electron transferred is = 309.46×10^{-3} C / 1.602×10^{-19} C

= 1.97×10^{18}

Since the reduction of Ni^{3+} to Ni^{2+} is a single electron transfer reaction, the number of electrons calculated above is the same as the number of surface active sites.

Hence, the surface-active Ni^{3+} sites participated in OER is = **1.97×10^{18}**

For S-NiFeOOH

Calculated area associated with the reduction peak = 5.5832 × 10^{-3} V A

Hence the associated charge is = 5.5832 × 10^{-3} V A / 0.005 V s^{-1}
= 1116.64 × 10^{-3} A s
= 1116.64 × 10^{-3} C

Now, the number of electron transferred is = 1116.64 × 10^{-3} C / 1.602 × 10^{-19} C
= 6.97 × 10^{18}

The surface-active Ni^{3+} sites participated in OER is = **6.97 × 10^{18}**

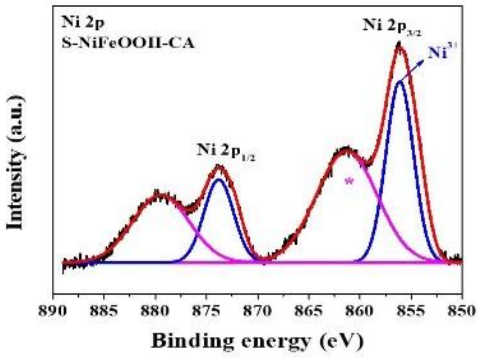


Figure 18: Ni 2p XP spectrum of S-NiFeOOH after 24 h OER-CA deconvoluted into two peaks at 856.14 eV and 873.81 eV, corresponded to Ni $2p_{3/2}$ and Ni $2p_{1/2}$, respectively. The peak at 856.22 eV was corresponded to the Ni^{3+} species while the * marked peaks were assigned for the satellite peaks [5-6].

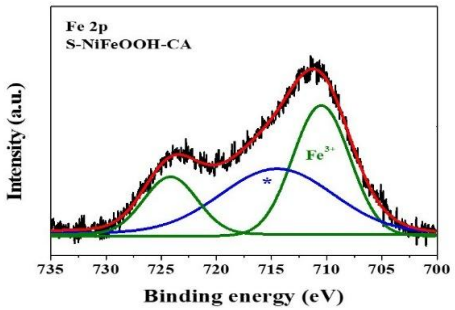


Figure 19: Fe 2p XP spectrum of S-NiFeOOH after 24 h OER-CA deconvoluted into two peaks at 711.21 eV and 723.86 eV, corresponded to Fe $2p_{3/2}$ and Fe $2p_{1/2}$, respectively. The peak at 710.50 eV was corresponded to the Fe^{3+} species while the * marked peaks were assigned for the satellite peaks [7-9].

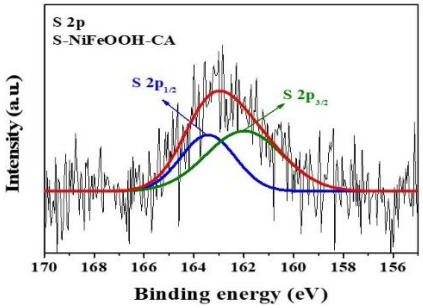


Figure 20: S 2p XPS spectrum of S-NiFeOOH after 24 h OER-CA showing two peaks at 162.00 eV and 163.45 eV for S $2p_{3/2}$ and S $2p_{1/2}$, respectively [10-11].

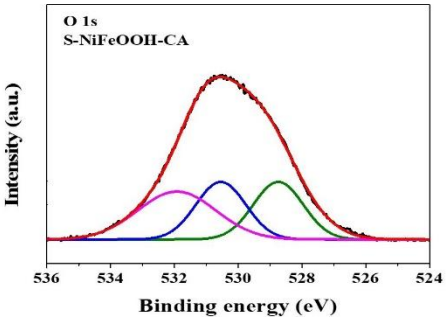


Figure 21: O 1s XPS of S-NiFeOOH after 24 h OER-CA deconvoluted into three peaks at binding energies 528.78 eV, 530.59 eV, and 531.96 eV corresponded to M-O and surface –OH groups, and adsorbed water molecules, respectively [10-11]

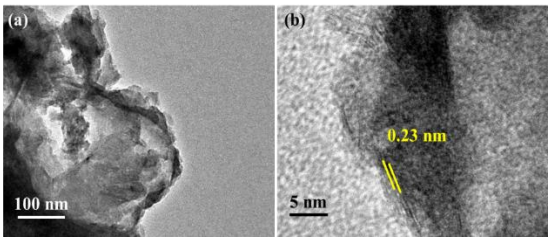


Figure 22: (a) TEM image of S-NiFeOOH after 24 h OER-CA indicating the ultrathin nanosheet morphology and (b) HRTEM image of S-NiFeOOH after 24 h OER-CA showing the d-spacing of 0.23 nm assigned for the (101) plane of α-$Ni(OH)_2$ (JCPDS No-38-0175).

11. Conclusion

In conclusion, the exploration of S-Doped NiFeOOH electrocatalysts reveals their pivotal role in advancing sustainable energy solutions, particularly in the realm of water splitting. As the world grapples with the pressing need for clean and renewable energy sources, the significance of these materials cannot be overstated. S-Doping enhances the electrochemical properties of NiFeOOH, improving its catalytic efficiency and stability under operational conditions. This enhancement not only facilitates more effective water dissociation but also contributes to the overall efficiency of hydrogen production, a clean fuel with the potential to power a myriad of applications.

The findings underscore the importance of tailoring electrocatalysts to optimize their performance for specific applications. S-Doped NiFeOOH stands out as a promising candidate due to its abundant availability, low cost, and remarkable electrochemical characteristics. As researchers continue to refine these materials and explore new doping strategies, the potential for scalable and economically viable hydrogen production becomes increasingly tangible.

Ultimately, the integration of S-Doped NiFeOOH into water-splitting technologies could serve as a cornerstone in the transition to a more sustainable energy future, reducing our reliance on fossil fuels and minimizing environmental impact. Embracing such innovative solutions is essential for addressing the global energy crisis and fostering a cleaner, greener planet for generations to come

References

[1] A. Higareda, D. L. Hernández-Arellano, L. C. Ordoñez, R. Barbosa and N. Alonso-Vante, *Catalysts*, DOI:10.3390/catal13101346.
[2] J. Ran, J. Yu and M. Jaroniec, *Green Chem.*, 2011, **13**, 2708–2713.
[3] P. H. Cyril and G. Saravanan, *New J. Chem.*, 2020, **44**, 19977–19995.
[4] E. Amores, M. Sánchez, N. Rojas and M. Sánchez-Molina, *Sustain. Fuel Technol. Handb.*, 2020, 271–313.
[5] J. Luo, J. H. Im, M. T. Mayer, M. Schreier, M. K. Nazeeruddin, N. G. Park, S. D. Tilley, H. J. Fan and M. Grätzel, *Science (80-.).*, 2014, **345**, 1593–1596.
[6] Y. Hou, M. R. Lohe, J. Zhang, S. Liu, X. Zhuang and X. Feng, *Energy Environ. Sci.*, 2016, **9**, 478–483.
[7] J. Li, J. Song, B. Y. Huang, G. Liang, W. Liang, G. Huang, Y. Qi Jin, H. Zhang, F. Xie, J. Chen, N. Wang, Y. Jin, X. B. Li and H. Meng, *J. Catal.*, 2020, **389**, 375–381.
[8] Y. Wu, H. Wang, S. Ji, X. Tian, G. Li, X. Wang and R. Wang, *Appl. Surf. Sci.*, 2021, **564**, 150440.
[9] J. Hu, S. Li, J. Chu, S. Niu, J. Wang, Y. Du, Z. Li, X. Han and P. Xu, *ACS Catal.*, 2019, 10705–10711.
[10] W. Wang, X. Xu, W. Zhou and Z. Shao, *Adv. Sci.*, , DOI:10.1002/advs.201600371.
[11] M. Shumba and T. Nyokong, *Electroanalysis*, 2016, **28**, 3009–3018.
[12] I. M. Patil, V. Reddy, M. Lokanathan and B. Kakade, *Appl. Surf. Sci.*, 2018, **449**, 697–704.
[13] R. Yadav and N. K. Singh, *Indian J. Chem. Technol.*, 2018, **25**, 189–195.
[14] J. Fan, X. Qin, W. Jiang, X. Lu, X. Song, W. Guo and S. Zhu, *Front. Chem.*, 2022, **10**, 1–10.
[15] S. Dutta, A. Indra, Y. Feng, T. Song and U. Paik, *ACS Appl. Mater. Interfaces*, 2017, **9**, 33766–33774.
[16] J. Mohammed-Ibrahim, *J. Power Sources*, 2020, **448**, 227375.
[17] M. Kumar and R. P. Singh, 2024, **13**, 1446–1451.
[18] M. Kumar and R. P. Singh, 2024, **13**, 313–319.
[19] M. Kumar and R. P. Singh, 1–16.
[20] A. Maiti and S. K. Srivastava, *J. Mater. Chem. A*, 2018, **6**, 19712–19726.
[21] P. Shi, X. Cheng and S. Lyu, *Chinese Chem. Lett.*, 2021, **32**, 1210–1214.
[22] X. Liu, Z. Chen and M. Cao, *ACS Appl. Energy Mater.*, 2019, **2**, 5960–5967.
[23] P. Li, X. Duan, Y. Kuang, Y. Li, G. Zhang, W. Liu and X. Sun, *Adv. Energy Mater.*, 2018, **8**, 1–8.
[24] Y. Feng, X. Y. Yu and U. Paik, *Sci. Rep.*, 2016, **6**, 1–8.
[25] P. Prieto, V. Nistor, K. Nouneh, M. Oyama, M. Abd-Lefdil and R. Díaz, *Appl. Surf. Sci.*, 2012, **258**, 8807–8813.
[26] A. Indra, M. Greiner, A. K. Gericke, R. Schlögl, D. Avnir and M. Driess, *ChemCatChem*, 2014, **6**, 1935–1939.
[27] S. Dey, B. Singh, S. Dasgupta, A. Dutta, A. Indra and G. K. Lahiri, *Inorg. Chem.*, 2021, **60**, 9607–9620.
[28] P. W. Menezes, A. Indra, P. Littlewood, C. Göbel, R. Schomäcker and M. Driess, *Chempluschem*, 2016, 81, 370–377.
[29] M. Wahlqvist and A. Shchukarev, *J. Electron Spectros. Relat. Phenomena*, 2007, **156**–**158**, 310–314.
[30] A. A. Wani, M. M. Bhat, F. A. Sofi, S. A. Bhat, P. P. Ingole, N. Rashid and M. A. Bhat, *New J. Chem.*, 2021, 45, 15544–15554.
[31] F. Song, G. Zan, Y. Chen, Q. Wu and Y. Xu, *J. Alloys Compd.*, 2018, **741**, 633–641.
[32] L. Cai, J. Zhao, H. Li, J. Park, I. S. Cho, H. S. Han and X. Zheng, *ACS Energy Lett.*, 2016, **1**, 624–632.
[33] X. Chen, Q. Wang, Y. Cheng, H. Xing, J. Li, X. Zhu, L. Ma, Y. Li and D. Liu, *Adv. Funct. Mater.*, , DOI:10.1002/adfm.202112674.
[34] Y. F. Yuan, X. H. Xia, J. B. Wu, J. L. Yang, Y. B. Chen and S. Y. Guo, *Electrochim. Acta*, 2011, **56**, 2627–2632.
[35] M. P. Suryawanshi, U. V. Ghorpade, S. W. Shin, U. P. Suryawanshi, E. Jo and J. H. Kim, *ACS Catal.*, 2019, **9**, 5025–5034.
[36] H. M. A. Amin, M. Attia, D. Tetzlaff and U. P. Apfel, *ChemElectroChem*, 2021, 8, 3863–3874.
[37] J. Baltrusaitis, D. M. Cwiertny and V. H. Grassian, *Phys. Chem. Chem. Phys.*, 2007, **9**, 5542–5554.
[38] T. Yamashita and P. Hayes, *Appl. Surf. Sci.*, 2008, **254**, 2441–2449.
[39] C. Long, L. Jiang, T. Wei, J. Yan and Z. Fan, *J. Mater. Chem. A*, 2014, **2**, 16678–16686.
[40] A. Indra, T. Song and U. Paik, *Adv. Mater.*, 2018, **30**, 1–25.
[41] B. Singh, O. Prakash, P. Maiti, P. W. Menezes and A. Indra, *Chem. Commun.*, 2020, **56**, 15036–15039.
[42] B. Singh, O. Prakash, P. Maiti and A. Indra, *ACS Appl. Nano Mater.*, 2020, **3**, 6693–6701.
[43] B. Singh and A. Indra, *Dalt. Trans.*, 2021, **50**, 2359–2363.
[44] B. Singh, A. K. Patel and A. Indra, *Mater. Today Chem.*, 2022, **25**, 1–24.
[45] H. Wang, H. S. Casalongue, Y. Liang and H. Dai, *J. Am. Chem. Soc.*, 2010, **132**, 7472–7477.
[46] H. Su, X. Zhao, W. Cheng, H. Zhang, Y. Li, W. Zhou, M. Liu and Q. Liu, *ACS Energy Lett.*, 2019, **4**, 1816–1822.
[47] B. Chen, Z. Yang, Q. Niu, H. Chang, G. Ma, Y. Zhu and Y. Xia, *Electrochem. commun.*, 2018, **93**, 191–196.